

Gold Nanoparticles Reduce Food Sensation in *Caenorhabditis elegans* via the Voltage-Gated Channel EGL-19

Meimei Wang^{1,*}, Zhenzhen Zhang^{2,*}, Ning Sun³, Baolin Yang⁴, Jihao Mo⁵, Daping Wang², Mingqin Su¹, Jian Hu¹, Miaomiao Wang⁶, Lei Wang^{7,8}

¹Department of Pathophysiology, School of Basic Medical Science, Anhui Medical University, Hefei, Anhui, 230032, People's Republic of China; ²Department of Biomedical Engineering, Southern University of Science and Technology, Shenzhen, 518055, People's Republic of China; ³Institute of Clinical Laboratory Science, Jinling Hospital, School of Medicine, Nanjing University, Nanjing, Jiangsu, 210002, People's Republic of China; ⁴Institute of Technical Biology & Agriculture Engineering, Hefei Institutes of Physical Science, Chinese Academy of Sciences, Hefei, Anhui, 230032, People's Republic of China; ⁵Department of Medical Laboratory, Luoyang Orthopedic Hospital of Henan Province, Orthopedic Institute of Henan Province, Luoyang, Henan, 459001, People's Republic of China; ⁶School of Medical Science, Huang He Science and Technology University, Zhengzhou, Henan, 459001, People's Republic of China; ⁷School of Biological Sciences, Nanyang Technological University, Singapore, 639798, Singapore; ⁸Department of Physiology and Biophysics, Miller School of Medicine, University of Miami, Miami, FL, 33136, USA

*These authors contributed equally to this work

Correspondence: Lei Wang, Department of Physiology and Biophysics, Miller School of Medicine, University of Miami, Miami, FL, 33136, USA, Tel +1 786-620-1400, Email lxw561@miami.edu

Introduction: The increasing use of gold nanoparticles (Au NPs) in the medical field has raised concerns about the potential adverse effect of Au NPs exposure. However, it is difficult to assess the health risks of Au NPs exposure at the individual organ level using current measurement techniques.

Methods: The physical and chemical properties of Au NPs were characterized by transmission electron microscope (TEM), Fourier transform infrared (FTIR), and zeta sizer. The RNA-seq data of Au NPs-exposed worms were analyzed. The food intake was measured by liquid culture and Pharyngeal pumping rate. The function of the smell and taste neurons was evaluated by the chemotaxis and avoidance assay. The activation of ASE neurons was analyzed by calcium imaging. The gene expression of *ins-22* and *egl-19* was obtained from the *C. elegans* single cell RNA-seq databases.

Results: Our data analysis indicated that 62.8% of the significantly altered genes were functional in the nervous system. Notably, developmental stage analysis demonstrated that exposure to Au NPs interfered with animal development by regulating foraging behavior. Also, our chemotaxis results showed that exposure to Au NPs reduced the sensation of *C. elegans* to NaCl, which was consistent with the decrease in calcium transit of ASEL. Further studies confirmed that the reduced calcium transit was dependent on voltage-gated calcium channel EGL-19. The neuropeptide INS-22 was partially involved in Au NPs-induced NaCl sensation defect. Therefore, we proposed that Au NPs reduced the calcium transit in the ASEL neuron through *egl-19*-dependent calcium channels. It was partially regulated by the DAF-16 targeting neuropeptide INS-22.

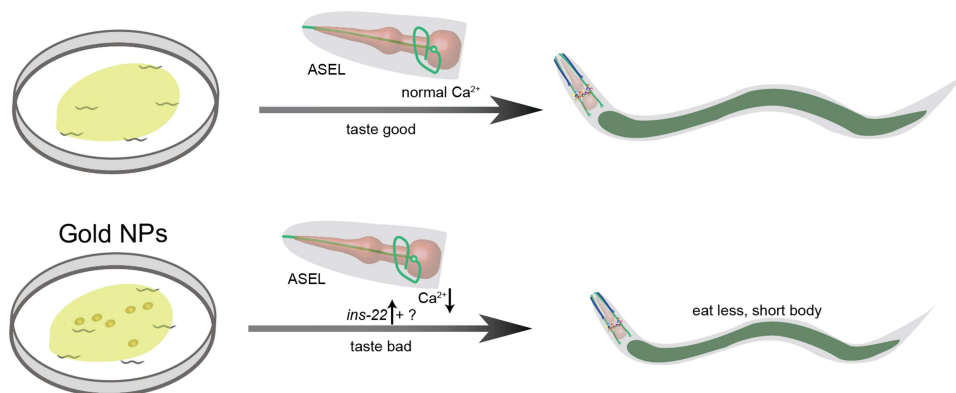
Discussion: Our results demonstrate that Au NPs affect food sensation by reducing the calcium transit in ASEL neurons, which further leads to reduced pharynx pumping and feeding defects. The toxicology studies of Au NPs from worms have great potential to guide the usage of Au NPs in the medical field such as targeted drug delivery.

Keywords: gold nanoparticles, RNA sequencing, ASEL neuron, voltage-gated calcium channel, developmental toxicity, *Caenorhabditis elegans*

Introduction

Au NPs have become one of the most studied nanomaterials in biomedical applications due to their physical/chemical stability and special optical properties. In recent decades, the interactions between engineered Au NPs and liver, kidney, blood vessels, and tumors have been studied.¹⁻⁴ Additionally, Au NPs can partially penetrate the blood-brain barrier in

Graphical Abstract



the brain, allowing them to function in the central nervous system.⁵ Targeted drug delivery using Au NPs has been tested in tumors, the liver, lung, and inhalation.^{6–9} Recent research showed specific modified Au NPs have antibacterial activity¹⁰ antioxidant activities,¹¹ and detect SARS-CoV-2.¹² Although relatively low toxicity has been reported on Au NPs, most researchers agree that exposure to nano-scale materials can lead to chronic toxicity, which may be due to the responses at the gene and protein level.^{13,14}

Biodistribution is a key factor in understanding how nanoparticles (NPs) accumulate and interact with each organ. Current quantification techniques require the isolation of each internal organ or the fluorescent/radio imaging modalities to modulate the entire animal. In addition to the biodistribution of the NPs, understanding how each organ responds to NPs in vivo is a huge challenge in humans, but it is possible in small animals. Studies on rabbits showed that 250 nm Polyethylene glycol (PEG) coated nanoparticles were mostly sequestered in the spleen and liver. However, 150 nm PEG coated nanoparticles were mostly found in the bone marrow.¹⁵ The inhalation rat model showed that silver (Ag) NPs was accumulated in lung, liver, brain, the olfactory bulb, kidney, and spleen.^{16–18} The laser-synthesized TiN NPs were mainly accumulated in the liver and spleen.¹⁹ Au NPs show a similar biodistribution trend as PEG coated NPs or AgNPs. Studies on mice have shown that 13 nm Au NPs coated with PEG were mainly deposited in the liver, kuffer cells, and spleen.^{20,21} While some studies on rats have shown that 18 nm Au NPs accumulated in the liver and spleen, 1.4 nm NPs were mainly in the kidney.²² The intestine of *C. elegans*, has the combined function of the liver, spleen, and kidney, accumulating most of the Au NPs.²³ Although these organs accumulate Au NPs, how each organ responds to the Au NPs and how the expression of genes in each tissue restores homeostasis is still largely unknown.

Although Au NPs did not accumulate in the nervous system, evidence has been reported that Au NPs modulate neural activity in multiple nervous systems.^{24,25} It has been shown that Au NPs increase neurite length, promote adhesion and proliferation, change the action potentials, and affect Ca²⁺ influx.^{26–28} Furthermore, engineered Au NPs were able to bind to sodium channels, transient receptor potential vanilloid member 1 channels, and P2X3 receptor ion channel in dorsal root ganglion neurons, thereby affecting the neuron–neuron communication.²⁵

Despite the numerous in vivo and in vitro cytotoxicity studies that have been studied on Au NPs, the results vary depending on the cell type used, exposure time, the physical and chemical properties, and the surface modification of nanomaterials. In vitro studies using human oral cancer cells (HSC-3) have demonstrated that Au NPs enter the cytoplasm, mitochondria, and nucleus. Few publications claim toxicity of Au NPs at a lower concentration than 1 ppm.²⁹ However, when increased to 10 ppm or higher, increased expression of apoptosis, oxidative stress, and pro-inflammatory genes was reported.³⁰ Apoptosis, autophagy, DNA damage, and necrosis were also observed in HSC-3, HeLa cells, and BALB/c mice liver studies.^{31–33} Furthermore, it has been shown that the higher levels of oxidative stress generated by the large surface of Au NPs could cause DNA and Mitochondrial damage, further destroying cellular homeostasis.³²

C. elegans is a small transparent animal with multiple important signaling pathways conserved in mammals, like autophagy, insulin, and apoptosis signaling pathways.³⁴ Here, we analyzed RNA sequencing data from Au NPs-exposed worms. However, different from the biodistribution data, the results indicated that the nerve system was the most affected when *C. elegans* were exposed to Au NPs. Further studies showed that the neuropeptide INS-22, a target gene of the transcription factor DAF-16, partially regulates the loss of food sensation induced by Au NPs. The calcium transit analysis indicated that the ASEL neurons reduced the calcium transit induced by Au NPs, which could be the way how Au NPs affect food sensation.

Materials and Methods

Characterization of Au NPs

Au NPs (40 nm) were purchased from Biotech (Jieyi, Shanghai). NPs were suspended in Milli-Q water (Millipore, 18M Ω cm), and then diluted in S medium (1L H₂O, 5.85g NaCl, 1g K₂HPO₄, 6g KH₂PO₄, 10mL 1M potassium citrate pH6, 0.0186g disodium EDTA, 0.0069g FeSO₄·7H₂O, 0.002g MnCl₂·4H₂O, 0.0029g ZnSO₄·7H₂O, 0.00025g CuSO₄·5H₂O, 3mL 1M CaCl₂, 3mL 1 M MgSO₄), as detailed in supplementary appendix. All NPs suspensions were sonicated for 30 minutes before the following experiments. The TEM images were obtained using a transmission electron microscope Tecnai G2-12. Briefly, the diluted Au NPs solution was dropped onto carbon-coated copper grids and then dried at room temperature. At least 6 locations on the grid were measured as described.³⁵ The diameter was calculated considering a perfectly spherical shape by Fiji Image J. The FTIR samples were prepared as previously described.^{36,37} The FTIR spectroscopy of the sample was taken in the region between 0 and 4300 cm⁻¹ (with Bruker, Alpha-T, USA). The size distribution and zeta potential were tested by a Malvern zeta sizer (HTS3000, Germany).

Nematode Maintenance and Exposures

All the nematode strains were obtained from the Caenorhabditis Genetics Center (St. Paul, MN) and listed in [Table S1](#). The synchronized worms were cultured on nematode growth medium (NGM) agar plates seeded with *Escherichia coli* OP50 at 20°C according to standard methods.³¹⁻³³ The *F45D3.2*, *gst-39*, and *W02B12.1* knockdown strains were generated by RNAi feeding as described.³⁸ P0 synchronized worms were exposed to Au NPs prepared in S basal liquid medium till they reach the young adults' stage.

Measurement of Body Length and Developmental Stage

Briefly, the wild-type worms were let grow on NGM plates for 3 days. Then the adult worms were bleached to get the synchronized L1 worms. After that, the synchronized worms were cultured in NGM plates containing OP50 with 0, 1, 10, and 100 μ g/mL of Au NPs, respectively. The worms were observed every 24 hours. Animals were anesthetized by 100 mM sodium azide on slides. The images were taken by Leica microscope with a 10 \times objective lens and the body length was measured by Image J. The developmental stage was determined by observing the phenotype of each organ and the body length as described.³⁹ At least 100 worms were counted for each condition. The graph was generated by R studio. The data in the manuscript were labeled as average \pm standard error.

Measurement of Pharyngeal Pumping

The pharyngeal pumping rate was quantified by analyzing the 60-second video recording of the contraction of the pharyngeal bulb. The videos were recorded with a Dino-eye Eyepiece camera (Dino-eye, Taiwan) mounted on a stereomicroscope (Nikon, Tokyo). The contractions were carefully counted by monitoring the videos at 0.4 X playback speed as previously described.⁴⁰ Worms contracted less than 5 times per 10 seconds were considered as non-pumping and were excluded from the experiments.

Measurement of Food Intake

The amount of bacteria intake was measured as previously described.³⁸ Briefly, the food intake of live bacteria was measured by quantification of the fluorescence intensity of *E. coli* GFP in vivo. The young adult worms were transferred to NGM plates containing fresh OP50-GFP with or without Au NPs for 24 hours culture. Then the worms were rinsed 3

times and resuspended in M9 buffer (3 g KH_2PO_4 , 6 g Na_2HPO_4 , 5 g NaCl, 1 mL 1 M MgSO_4 , H_2O to 1000 mL) for 15 minutes to wash off any *OP50*-GFP that might be attached to the body wall. Worms were immobilized with 100 mM NaN_3 and mounted on 2% agarose pad. Images were captured using Zeiss LSM 800 confocal microscope with a 20 X HC PL objective lens. At least 20 nematodes were recorded for each group. The consumption of dead *OP50* by worms was assessed in 96-well plates. Each well contains 5 to 10 young adult worms with 3 mg/mL of autoclave-killed *OP50* in 150 μL S-complete liquid medium plus 50 $\mu\text{g}/\text{mL}$ carbenicillin with or without Au NPs. The plates were shaken at 200 rpm for 15 mins and the absorbance at 600 nm was measured after 24 hrs incubation. The relative number of bacteria consumed was calculated by using the original absorbance at 600 nm to minus the absorbance at 600 nm after incubation and then normalized to the number of worms. The media with 50 $\mu\text{g}/\text{mL}$ carbenicillin and 3 mg/mL of autoclaving killed *OP50* with or without Au NPs was set as blank. At least 50 worms were recorded for each condition.

RNA Sequencing Data Analysis

RNA sequencing data of *C. elegans* exposed to Au NPs (GSE32521) was downloaded from Gene Expression Omnibus (GEO), National Center for Biotechnology Information (NCBI).⁴¹ Age-synchronized L3 worms were exposed to Au NPs at a concentration of 5.9 mg/L in 50% K-Medium (1.23 g NaCl, 0.968 g KCl, H_2O to 400 mL) for 12 hours, as detailed in the supplementary appendix. Then, they were cultured with 50% K-Medium and left for another 12h. The RNA was extracted from each of the replicates. Significantly changed genes with 1.5-fold and $p < 0.05$ and $\text{FDR} < 0.1$ were analyzed. The RNA sequencing data of *daf-16* target genes, reference series GSE1762, was obtained from GEO.⁴² The comparison between *daf-2* (*e1370*) and the double mutant *daf-2* (*e1370*); *daf-16* (*df50*) was used to determine the target genes for transcription factor DAF-16. The single-cell sequencing data for all the ciliated neurons were obtained from VisCello.⁴³ The data for all the sensory neurons were plotted using the log₁₀ value of raw read numbers per million by R using package *fmsb*.

Gene Expression Analysis

The $-\log_{10}$ P value and the log₂ fold change of each gene were plotted by package *ggplot2* Of R (version 3.5.2) to generate the volcano plot. The cutoff was set as fold change more than 1.5-fold and $p < 0.05$. For the genes with were 1.5-fold higher or lower expressed were marked in red. Gene expressions with less than 1.5-fold and $p > 0.05$ were marked in blue. The tissue enrichment was measured by Gene Set Enrichment Analysis.⁴³ The sub-tissues were set as the same color as the major tissue. The Au NPs specific motif sequence was obtained using the motif discovery tool.⁴³ The 5000 bp before ATG of each enriched genes were selected as the promoter sequence input. The enriched motifs length was set between 6 and 50 bp.

Measurement of Neuron Numbers

The number of neurons was quantified by counting the number of GFP-expressed cells in the *otIs672* [*rab-3*::NLS::GCaMP6s + *arrd-4*::NLS::GCaMP6s] strain. This strain has an ultra-pan-neuronal promoter containing four short pan-neuronal promoters fused. The worms were let grow to L4 stage, and then seeded to the 60 mm NGM plates containing *OP50* with or without 100 mg/L Au NPs for 24 hours. At last, the worms were mounted on slides with sodium azide for imaging. The images were taken by Leica fluorescence microscope with a 20X objective lens as described. The cells with clear nucleus localization were counted and plotted by GraphPad 8.

Subcellular Localization of DAF-16

The subcellular localization of DAF-16 indicates the activation of insulin like receptor pathway. The *daf-16p*::*daf-16a/b*::GFP worms were let grow to L4 stage, then seeded to the 60 mm NGM plates containing *OP50* with or without 100 mg/L Au NPs for 24 hours. Lastly, the worms were mounted on slides with sodium azide for imaging. The worms of positive control group were exposed to 37°C for 1 hour. The images were taken by a Leica fluorescence microscope with 20X objective lens. The number of cells with clear nucleus localization was counted as previously described⁴⁰ and plotted by Graphpad 8. The data in the graph was labeled as average \pm standard error.

Chemotaxis Assay

The chemotaxis assays were proceeded according to standard procedures as previously described.^{40,44–47} For isoamyl alcohol and diacetyl assays, 3 μ L of odor at the indicated dilution was placed on one side of the plate. Three μ L of the solvent ethanol was added to the other side of the plate. For NaCl assays, a chunk of agar around 1cm in diameter was removed from 10cm plates and soaked in the 0.2 M of NaCl for 3 hours. The chunks were put back in the plate overnight to allow the formation of a NaCl gradient. Fifty μ L of 100 mM NaN₃ were placed on both the control and the test spots to anesthetize animals once they reached the spot. The control group and 100 μ g/mL Au NPs pre-exposed worms were placed in the middle of the 10 cm plate. The attraction index was calculated using the equation $AI = (B-A)/(A+B)$. For 1-octanol assay, the worms were placed in a NGM plate with a thin layer of *OP50*. We dipped an eyelash hair tapped on a 1 mL tip and put in front of a forward moving worm. Then, we count the seconds of the animal starts backward movement as a result of responding to the octanol. The worm needs more than 10 seconds to response before it is considered unresponsive. All the assays were performed blind to the conditions.

The Morphology of ASEL and ASER Neurons

The morphology of ASEL and ASER neurons was monitored by using two strains that specifically expressed GFP in ASEL or ASER neurons. The young adult worms exposed to 0 or 100 mg/L Au NPs for 24 hours were anesthetized with 100mM sodium azide on glass slides covered with 2% agar. The optical section images were collected by EVOS FL auto 2 system using 20X, and 40X objective lens. The length of dendrite, the area of cilia and cell body were measured using Fiji Image J.⁴⁸

The Calcium Transit Assay

Calcium imaging recordings were performed in accordance with standard procedures with minor modifications.⁴⁹ Worms were immersed in bath solution containing 5 mM KPO₄ buffer, 1 mM MgSO₄, and 1 mM CaCl₂, adjusted to pH6.0, and glued to a 2% agar pad settled on a glass covers lip using medical glue. The NaCl bath buffer was the above buffer containing 20 mM NaCl. The buffer was delivered to a recording chamber via gravity perfusion with the speed of perfusion was 10 mL/min. Images were acquired using MicroManager 2.0 software⁵⁰ at a frequency of 1 Hz with 100 ms exposure time and a spatial resolution of 1024×1024 pixels. Basal fluorescence prior to exposure to the chemicals was acquired for 15 seconds. The perfusion with the NaCl was for 20 seconds, followed by washing with the bath solution until the end of the recording. The fluorescence intensity was calculated by subtracting the background.

Protein's Function and Subcellular Localization Analysis

The genes which are significantly increased in expression are selected for the protein–protein function analysis. For the interactions, we analyzed co-expression, genetic interactions and physical interactions using Genemania.⁵¹ For the protein–protein interaction analysis, the top 20 genes which are significantly in expression were selected and analyzed by STRING.⁵²

Statistical Analysis

Statistical analysis with 3 groups or more was conducted using one-way ANOVA followed by Tukey's. Analysis with 2 groups was conducted using Student's test. The data were collected and graphed by ggplot2 package from R and GraphPad 8. Data are represented as mean \pm SEM obtained from at least three independent experiments. P values are represented as * p <0.05, ** p <0.01, *** p <0.001.

Results and Discussion

Characterization of Au NPs

The size of nanoparticles is a key factor affecting their absorption, distribution, and toxicity.^{53–56} Studies have shown that silica NPs (>80 nm) induced decreased cell viability and increased oxidative stress.⁵³ Smaller-sized silver NPs induce more severe apoptosis in mouse fibroblasts.⁵⁶ Uptake of 45 nm Au NPs has been reported to penetrate cells through clathrin-mediated endocytosis, whereas the smaller 13 nm enter cells mainly through phagocytosis.⁵⁵ Moreover, the smaller size of Au NPs reduced the colony formation efficiency of mouse fibroblasts.⁵⁴ Here, the size and coating characteristics were characterized by TEM and FTIR firstly. The TEM image showed the average size of the Au NPs was 26.67 ± 0.51 nm

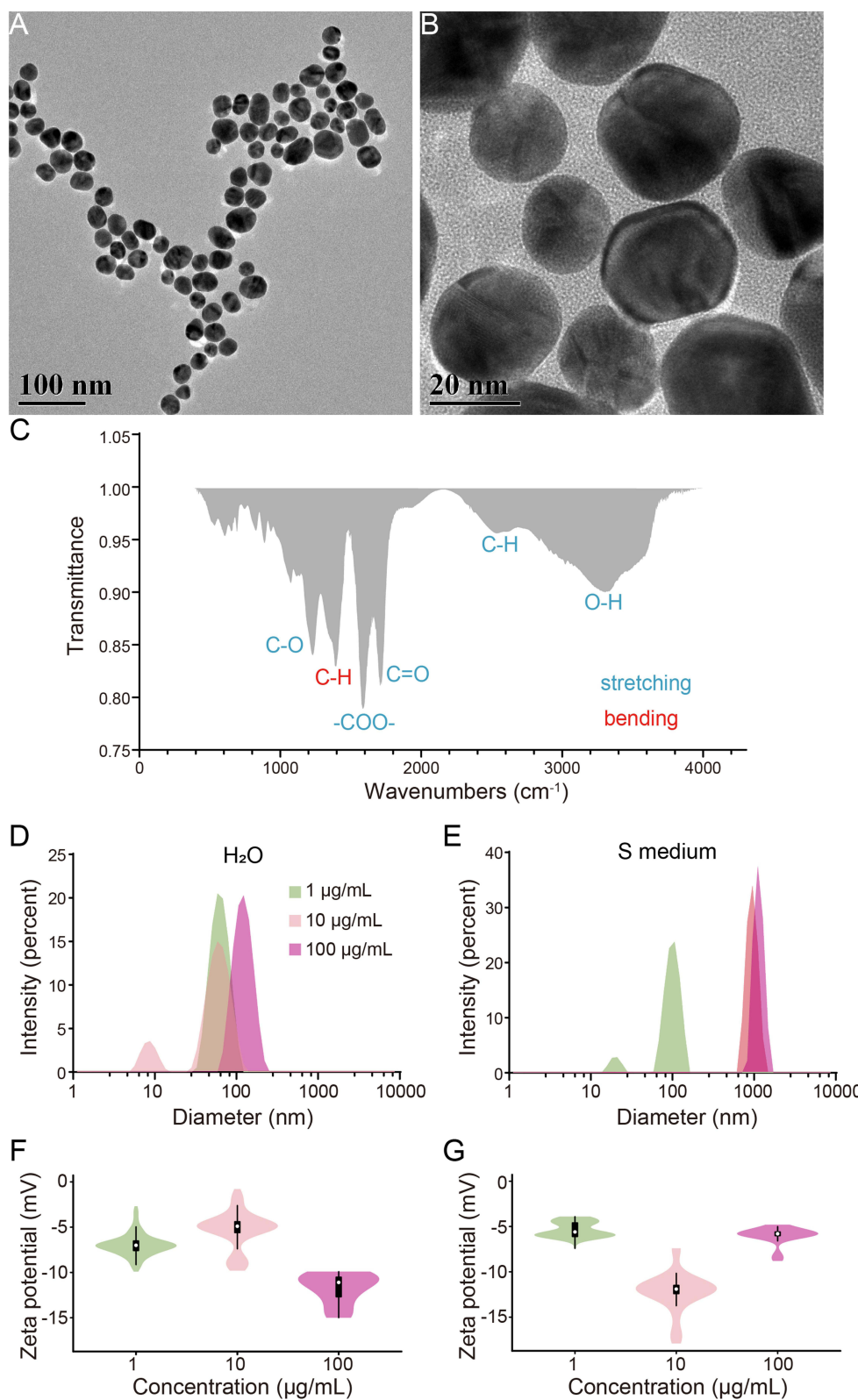


Figure 1 Characterization of Physicochemical properties of Au NPs and stability in water and S medium. **(A–B)** The TEM images of Au NPs. The scale bars represent 100 nm and 20 nm respectively. **(C)** FTIR of Au NPs. Stretching vibrations are labelled blue, bending vibration is labelled red. **(D–G)** Size distribution of 1, 10 and 100 μg/mL Au NPs in H₂O or S medium. Green represents the 1 μg/mL Au NPs group, lemonade represents the 10 μg/mL Au NPs group, magenta represents the 100 μg/mL Au NPs group. Data are shown as mean ± SE.

(Figure 1A and B). FTIR suggested that the Au NPs were coated with citric acid to aid distribution (Figure 1C). Further, to understand the status of Au NPs in the solvent, we analyzed the size distribution and zeta potential in water and S medium (Supplementary Appendix). As shown in Figure 1D and E, the hydrated size of Au NPs becomes larger with increasing concentration. However, the particle size of Au NPs at 10 and 100 mg/L did not differ significantly in S matrix medium, but there was a significant difference in the particle size in water (Figure 1D-G). Since the pH of S basal medium and water are very close, the possible explanation is the salt such as Fe^{2+} , Mn^{2+} , Zn^{2+} , Cu^{2+} , Cl^- , and SO_4^{2-} have impact on the aggregation of Au NPs. This is consistent with the observation that the aggregation of Au NPs in solution is influenced by cations and oligomers, which control the aggregation behavior of Au NPs. The zeta potentials for water and S basal medium are relatively consistent for three different concentrations. These results indicated that the size of Au NPs in S basal medium was larger than that in water, but the dispersion is stable after sonication.

Au NPs Delayed the Development of *C. elegans* Through Reducing the Food Intake

Recent studies on the effects of Au NPs on development have shown that embryonic exposure of Au NPs leads to the formation of several malformations and affects eye development during early developmental stages of zebrafish.^{57,58} Functional analysis indicated that genes enriched in the nervous system were strongly associated with development. It is generally believed that exposure starts from early stage is more reasonable for study the developmental effects of Au NPs. Therefore, we started to test from the L1 stage for 60 hours, when the worms were young adults. As shown in Figure 2A and B, exposure to 10 and 100 mg/L Au NPs adversely influenced the early development of *C. elegans*. The average body length of 100 mg/L Au NPs-treated worms were around 30% short than control group. It is consistent to the measurement of developmental stage determination results (Figure 2C). For the worms fed with 10 mg/L Au NPs, 0.8% young adult observed compare to nearly 40% for control. For the fourth day of culture, less eggs observed in the 10 and 100 mg/L Au NPs plates than the 0 and 0.1 mg/L conditions (data not shown). These results indicated that Au NPs concentration higher than 10 mg/L will delay the development of *C. elegans*, and this phenomenon is in a concentration-dependent manner.

In view of the above findings, we hypothesized that the developmental defects might be related to foraging behavior. We tested the food intake of the worms with live *OP50*-GFP. By measuring the intensity of GFP, we observed that 100 mg/L Au NPs exposure caused a significant reduction of worms in food intake. To eliminate the possibility that Au NPs-treated *OP50* produced some by-products causing abnormal development, we repeated the food intake experiments with dead *OP50*. As shown in Figure 2D, food intake was also significantly reduced in worms exposed to 100 mg/L Au NPs. These results confirmed that developmental abnormality of *C. elegans* caused by 100 mg/L Au NPs exposure was not related to the status of *OP50*. To conclude, 100 mg/L Au NPs exposure adversely influences the development of *C. elegans* by reducing food intake.

Foraging Behavior of *C. elegans* Depends Largely on the Pumping of Pharynx

The pharynx works as a tubular pump, sucking food into the intestine, concentrating and grinding them up.⁵⁹ The nicotinic acetylcholine receptor *eat-2* is necessary for rapid pharynx pumping.⁶⁰ *Eat-2* initiates the firing of motor neurons required for pumping action potential. Without *eat-2*, the pumping speed dropped to 10% of original rate.⁶⁰ To determine whether changes in food intake were related to pumping rate, we analyzed body length and pumping rate of wild-type and *eat-2* mutants (Figure 2E and F). Different from the wild type worms, the control and Au NPs-exposed *eat-2* mutants did not change significantly in body length and pumping rate. The results suggested that the developmental abnormality in *C. elegans* caused by 100 mg/L Au NPs was associated with reduced food intake and pumping, which were dependent on nicotinic acetylcholine receptor *eat-2*.

The Nervous System is the Organ Most Affected by Au NPs

The bio-distribution analysis of Au NPs accumulation in mice showed that the liver and spleen are the organs with most Au NPs accumulated.^{22,61,62} In *C. elegans*, there is no liver and spleen, but the intestine has the combined function of spleen, liver, kidney, and stomach. It is consistent with the observation in mice; the intestine has most Au NPs accumulated in Au NPs fed worms.²³ Correspondingly, most toxicological studies on animal models of Au NPs exposure

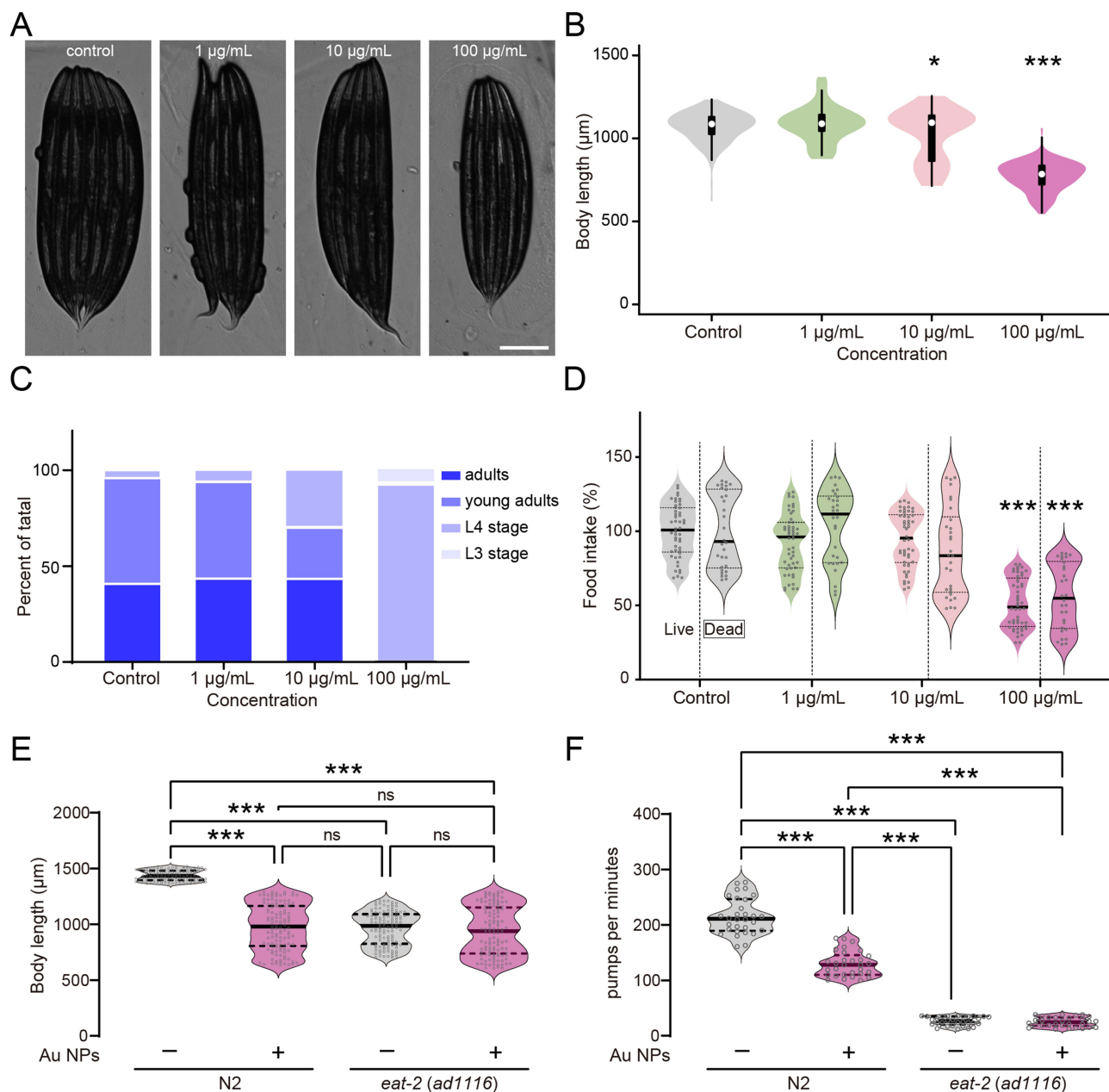


Figure 2 Au NPs induce development abnormality by reducing food intake. Images and body length quantification of worms exposed to 0, 1, 10 and 100 µg/mL Au NPs for 60 hours (A–B). Developmental stage analysis (C) and food intake measurement (D) of worms exposed to 0, 1, 10 and 100 µg/mL Au NPs. Body length analysis (E) and pumping rate quantification (F) of wild type and *eat-2* mutant worms exposed to 0 and 100 µg/mL Au NPs for 60 hrs. Gray represents the 0 µg/mL Au NPs group. Data are shown as mean ± SE. The “ns” represents not significant. P values are represented as *p < 0.05, ***p < 0.001.

were focused on the liver, spleen, and kidney.^{63–65} Indeed, the presence of Au NPs altered hepatic metabolism, such as increased aspartate aminotransferase (AST) level and decreased the level of gamma-glutamyl transferase (GGT), alanine transaminase (ALT) and alkaline phosphatase (ALP).⁶⁶ Furthermore, the transcriptome analysis of liver samples showed that Au NPs caused down-regulation of many cytochrome P450-related genes and up-regulation of inflammation-associated genes.⁶³

However, through analyzing the whole animal transcriptome, we found that the nervous system, instead of the intestine, was the organ with the most altered gene expression through Au NPs exposure in liquid culture (K-medium in supplementary appendix). By setting the cutoff at 1.5-fold change, we found a significant increase in nearly 800 genes and a significant decrease in 270 genes (Figure 3A). To analyze the organ-level mRNA expression induced by Au NPs,

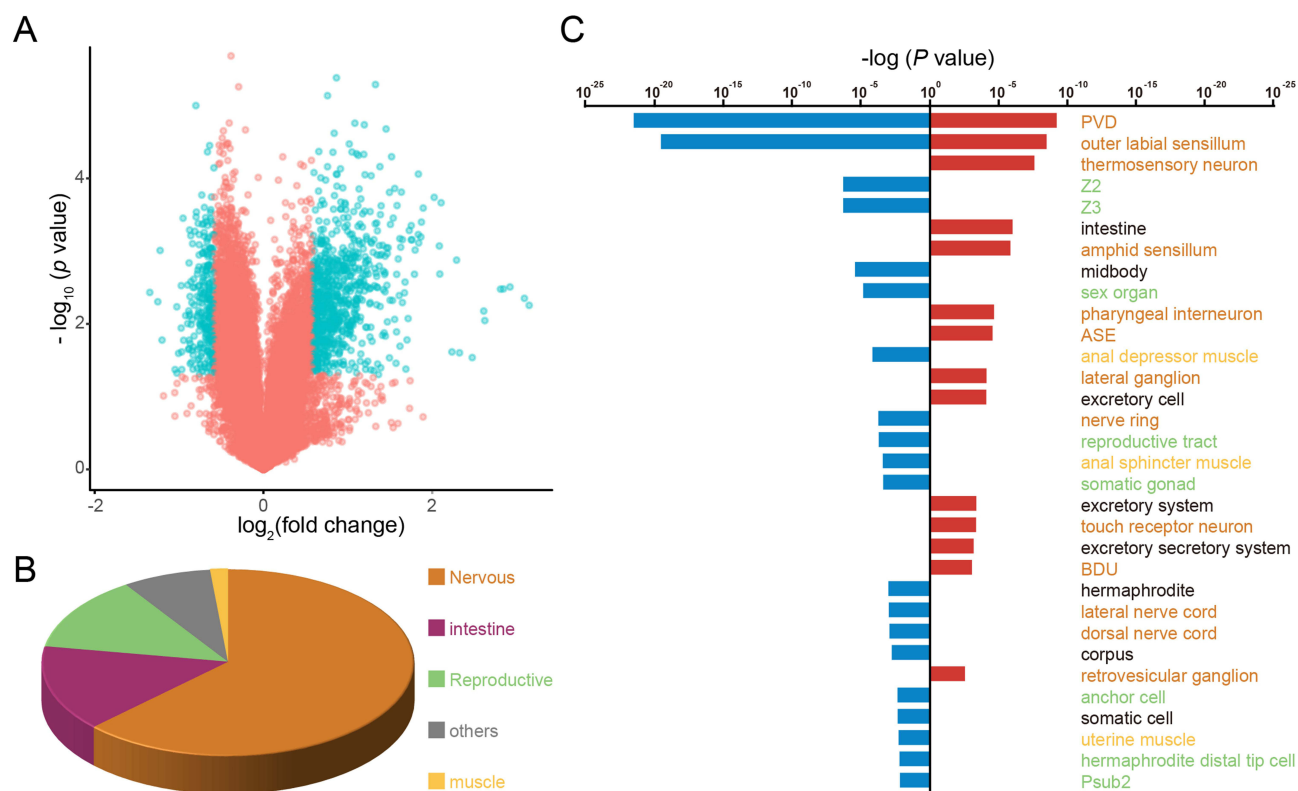


Figure 3 The nervous system is the main target organ for Au NPs treatment. **(A)** Volcano plot of expression changes of approximately 20,000 genes in *C. elegans* after Au NPs treatment. Each gene was plotted by fold change and *p*-value. Genes that have increased or decreased expression with fold change > 1.5 and *P* value < 0.05 are marked as blue hollow circles. Genes with increased or decreased expression for fold changes < 1.5 and *P* values > 0.05 are labeled as red hollow circles. Tissue enrichment analysis of genes that were significantly increased (blue) and decreased (red) in the Au NPs-exposed *C. elegans* group is shown by pie charts **(B)** and bar graphs **(C)**.

we performed tissue enrichment assays by inputting RNA-seq data. The results suggested that above 60% of the significantly altered genes were mainly functioning in the nervous system; around 15% were located to intestine, 8% in reproductive system, 15% in muscles and other tissues (Figure 3B). To check in detail, we investigated the sub-type of each category. For the nervous system, all its sub-type cells have both genes significantly up- and down-regulated, such as the outer labial sensillum. However, the intestinal cells show only up-regulated genes, the sub-types of reproductive system and muscle show only down-regulation (Figure 3C). To conclude, these results indicated that at transcriptome level, the nervous system is the major target organ of Au NPs.

To further elucidate the interaction of Au NPs with the nervous system at the mRNA expression level, we performed protein-protein interaction assays. We focused on the top 20 up-regulated genes and analyzed their functions based on their co-expression, gene interactions, physical interactions and shared protein structural domains. The functions of these genes were focused on cellular component organization, reproduction, multicellular organism development, nematode larval development, and embryonic development at birth or egg hatching (Figure S1A and B). These results are highly consistent with the results of gene ontology analysis, which also showed that Au NPs-induced changes in mRNA expression of neurological genes are highly correlated with development, such as larval, embryonic, reproductive and dendritic development (Figure S1C). In addition, we analyzed the specific binding pattern of Au NPs by using the promoter sequences of the upregulated genes as input. The results showed that a conserved 43 bp sequence was the specific binding pattern of Au NPs with an *e*-value of 1.5^{-222} (Figure S1D). Since our study was more focused on neuronal toxicity caused by Au NPs, we performed developmental stage assays based on functional analysis of neuronal genes. These results suggest that Au NPs exposure regulates development mainly through the regulation of gene function in the nervous system.

Au NPs Cause Defects in ASE Sensory Neuron's Function

Previous RNA sequencing data suggested that Au NPs induce gene changes mainly in the nervous system. To investigate whether changes in the gene expression cause any effect on neurons, we monitored the number of all neurons in *C. elegans*. As a result, we did not observe any change in the total number of neurons (Figure 4A-C). Since the foraging behavior of *C. elegans* was triggered by the sensation of food, we tested the function of each sensory neuron through chemotaxis assay (Figure 4D and E). As shown in Figure 4F-I, Au NPs-treated worms showed defects in NaCl sensation, but did not show any defect in IAA, diacetyl, and octanol sensation. These results suggested that the worms treated by Au NPs exhibited a defect in NaCl sensation, which indicated the functional defect in ASE. We know that defects in ASE neuron function could lead to the decrease in food intake and pumping rate.

Au NPs Lead to Decreased Calcium Transit in ASEL Neurons

It is well known that ASEL and ASER neurons control the sensation of NaCl, and calcium is an essential intracellular messenger in neurons. The Green fluorescent protein/Calmodulin sensor (GCaMP) can reflect changes in Ca^{2+} influx facilitated by stimulation-evoked neuronal action potentials. For example, the calcium transits of ASEL increase when the NaCl concentration changes from low to high. On the contrary, when the NaCl concentration changes from high to low, the calcium transport of ASER showed an increasing trend. In addition, neuronal morphology has been shown to be an important factor affecting neuronal function. Altered morphology can lead to changes in neuron function, which further affects their behavior.^{67,68} Here, to investigate the mechanism of NaCl sensation reduction in worms exposed to Au NPs, we observed morphology and measured neuronal function. Firstly, we measured the length of dendrite, the area of cilia and cell body of both ASEL and ASER neurons. The morphology of ASEL and ASER showed no change (Figure 5A-G). Then, we generated the ASE GCaMP strain (Table S1) and checked the function of ASEL neurons by measuring the calcium transit. As shown in Figure 5H and I, the max calcium transit was significantly reduced in Au NPs-treated worms. Figure S2 showed the calcium transit of each individual worm. However, we did not observe any changes in ASER neurons (Figure S3). The decay of ASEL calcium transit of Au NPs-treated worms lasted longer than wild type. These results indicated that Au NPs could induce decrease in ASEL calcium transit, leading to defect in food sensation.

Food Sensation Defects Caused by Au NPs Partly Depend on the Neuropeptide INS-22

It has been reported that the sensation and adaption of NaCl are largely dependent on the insulin/IGF-1 signaling (IIS) pathway.⁶⁹ Prolonged NaCl exposure did not increase Ca^{2+} responses of ASER in IIS pathway mutants as much as that in wild-type worms.⁷⁰ High concentrations of NaCl may induce developmental arrest by inhibiting the IIS signaling pathway, resulting in the activation of the FOXO transcription factor DAF-16.⁷¹ To test if Au NPs activate the IIS signaling pathway, we measured the subcellular localization of the transcription factor DAF-16 (Figure 6A and B). Compared with wild-type worms, the observed number of DAF-16 in nucleus was significantly increased. To investigate the specific genes that regulate NaCl sensation in ASEL neurons, we compared the transcriptome of DAF-16 dependent genes and Au NPs-ASEL-enriched genes. As a result, we found that 10 DAF-16 dependent genes are also enriched in Au NPs-ASEL genes (Figure 6C). We further studied the specific motifs recognized by DAF-16, which are present in the promoter regions of all 10 discovered genes (Figure 6D). To determine which gene regulates the NaCl sensation, we screened the mutants of DAF-16 dependent and Au NPs-ASEL enriched genes. Among all these mutants, the neuropeptide INS-22 mutant showed NaCl sensation defects (Figure 6E). By analyzing the single-cell RNA sequencing data of all the sensory neurons, we found that *ins-22* expression was enriched in ASEL, ASER, and AWC neurons (Figures 6F and S4). Studies have shown that the insulin-type neuropeptide INS-22 is more secreted during active reproductive stages,⁷² and it is usually secreted from dense core vesicles into the body cavity, where it is then taken up by coelomocytes.⁷³ To date, how INS-22 is involved in salt sensation remains largely unknown. Since it has been reported that AWC

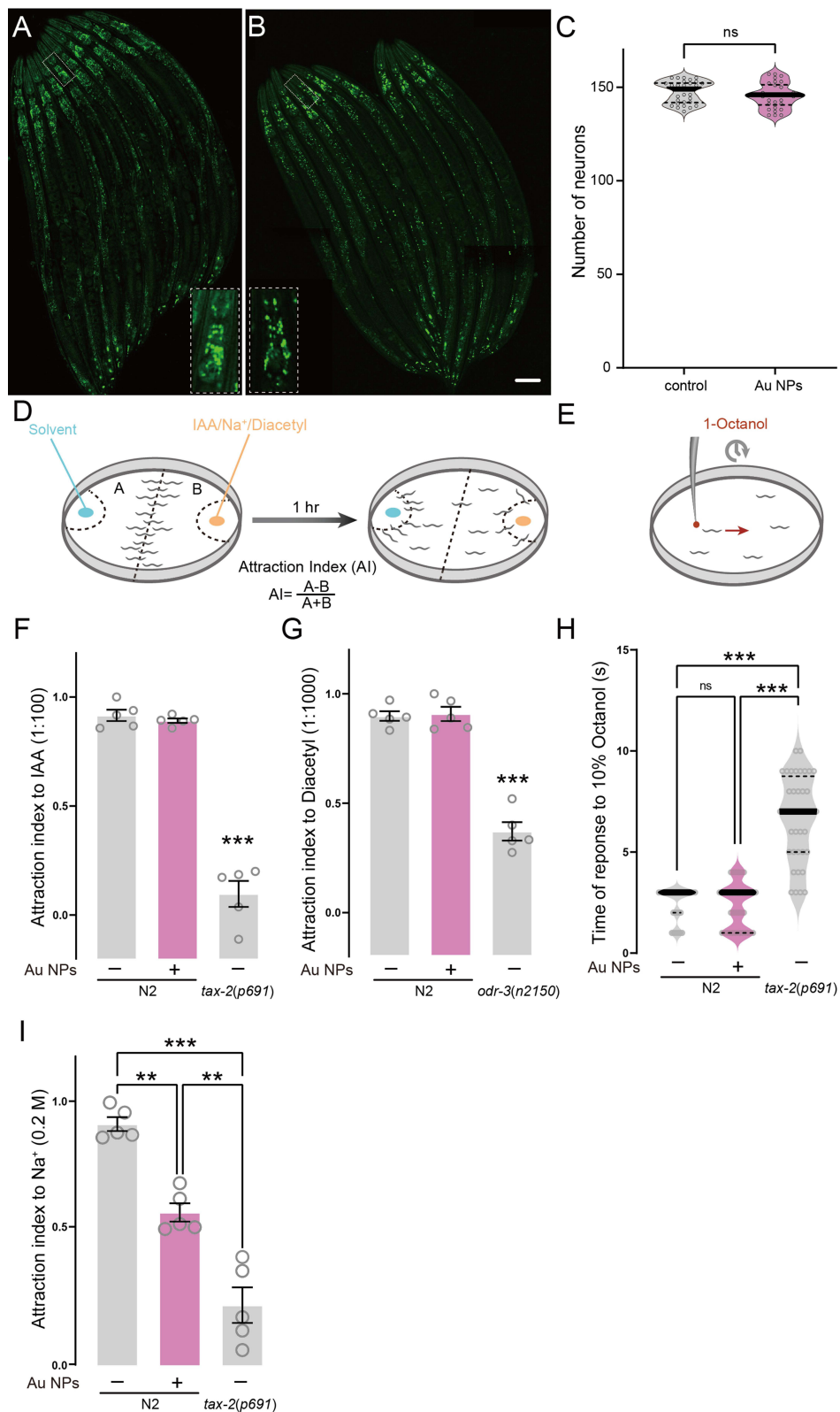


Figure 4 Au NPs-treated worms have decreased sensation of NaCl. (**A–B**) Images of all neurons in 0 and 100 $\mu\text{g/mL}$ Au NPs-exposed *C. elegans*. (**C**) The quantification of visible neuron numbers. (**D–E**) The cartoon for chemotaxis assay of IAA, NaCl, Diacetyl and 1-octanol. (**F–H**) The attraction index of 0 and 100 $\mu\text{g/mL}$ Au NPs-exposed worms to IAA, Diacetyl, and NaCl. (**I**) The response time of 0 and 100 $\mu\text{g/mL}$ Au NPs-exposed worms to 1-octanol. Gray represents the 0 $\mu\text{g/mL}$ Au NPs group, magenta represents the 100 $\mu\text{g/mL}$ Au NPs group. Data are shown as mean \pm SE. The “ns” represents not significant. P values are represented as ** $p < 0.01$, *** $p < 0.001$.

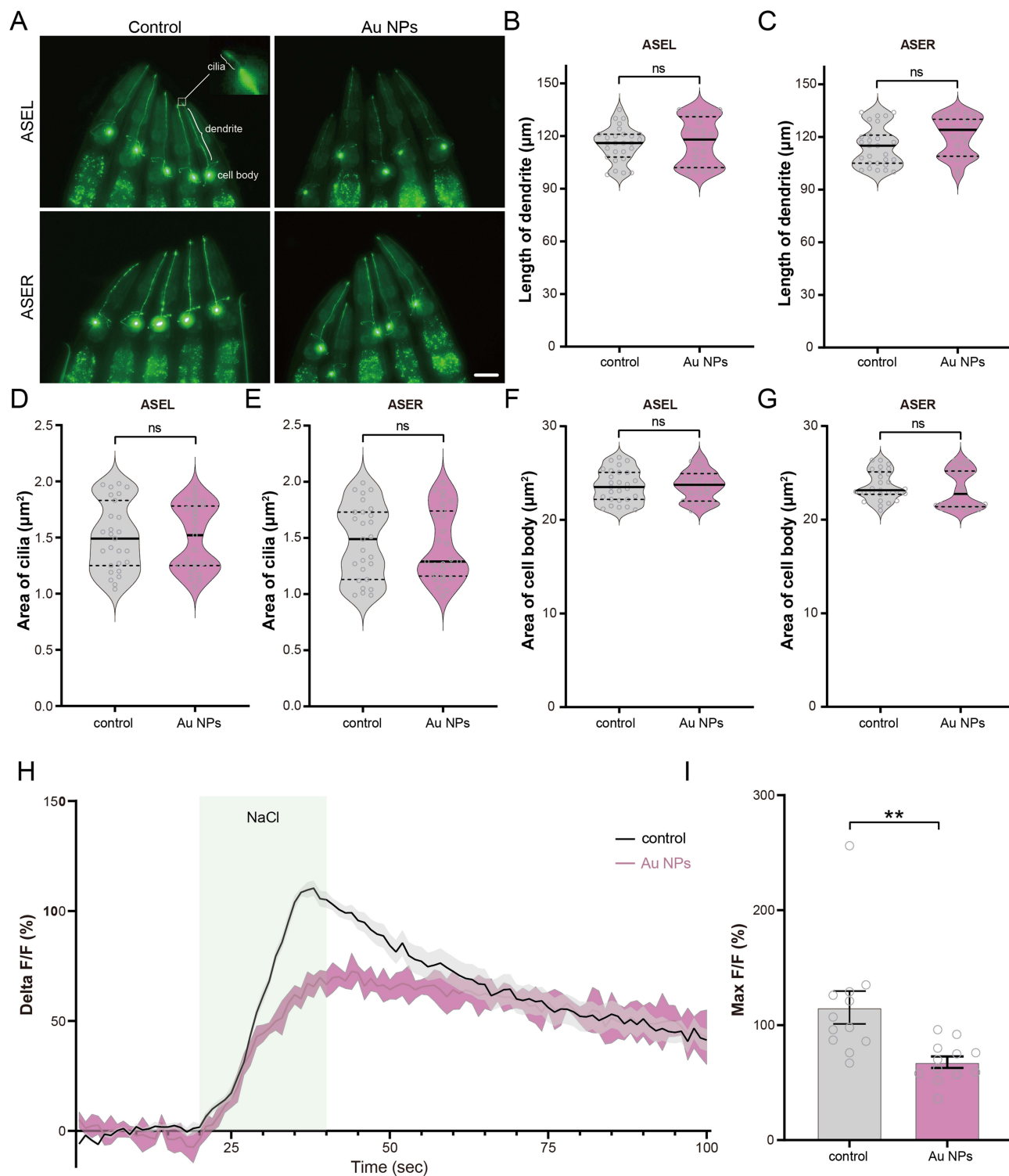


Figure 5 Au NPs exposure does not affect the morphology of ASEL and ASER neurons but decreases the calcium transit of ASEL. **(A)** The image of ASEL and ASER in 0 and 100 $\mu\text{g}/\text{mL}$ Au NPs-exposed worms. **(B–G)** The quantification of dendrite length, area of cilia, and area of cell body of ASEL and ASER neurons. **(H)** The calcium transit dynamics and **(I)** the max intensity of fluorescence signal of ASEL neuron of 0 and 100 $\mu\text{g}/\text{mL}$ Au NPs-pre-exposed worms to 20 mM NaCl. Gray represents the 0 $\mu\text{g}/\text{mL}$ Au NPs group, magenta represents the 100 $\mu\text{g}/\text{mL}$ Au NPs group. Data are shown as mean \pm SE. The “ns” represents not significant. P values are represented as ** $p < 0.01$.

neurons can act as inter-neuron for NaCl sensation,⁷⁴ we confirmed that *ins-22* is expressed in ASE and AWC neurons that sense NaCl. By testing the sensation of Au NPs-treated *ins-22* mutants to NaCl, we found that the attraction index of NaCl was significantly reduced (Figure 6G). Meanwhile, compared with Au NPs-treated wild-

type worms, the attraction index of NaCl in Au NPs-treated *ins-22* mutants significantly decreased. So, we hypothesize that INS-22 partially regulates the NaCl sensation defect induced by Au NPs.

Food Sensation Defects Caused by Au NPs Depend on EGL-19

The L-type voltage-gated calcium channel *egl-19* is essential for calcium transit in neurons and glial cells.^{75,76} Blocking or knockdown of *egl-19* induces decreases in calcium transit in ASE neurons.⁷⁷ EGL-19 cooperates with EAT-2 and CCA-1 to regulate the neuron functions and initiates the action potential in neurons and muscles.^{59,78} The expression of *egl-19* was observed in ASE, ASG, AWB, and other ciliated neurons (Figure S5). To confirm if *egl-19* was involved in Au NPs-induced pumping and NaCl sensation defects, we measured the pumping rate and attraction index of *egl-19* mutants. To elucidate the role of *egl-19* in Au NPs-induced

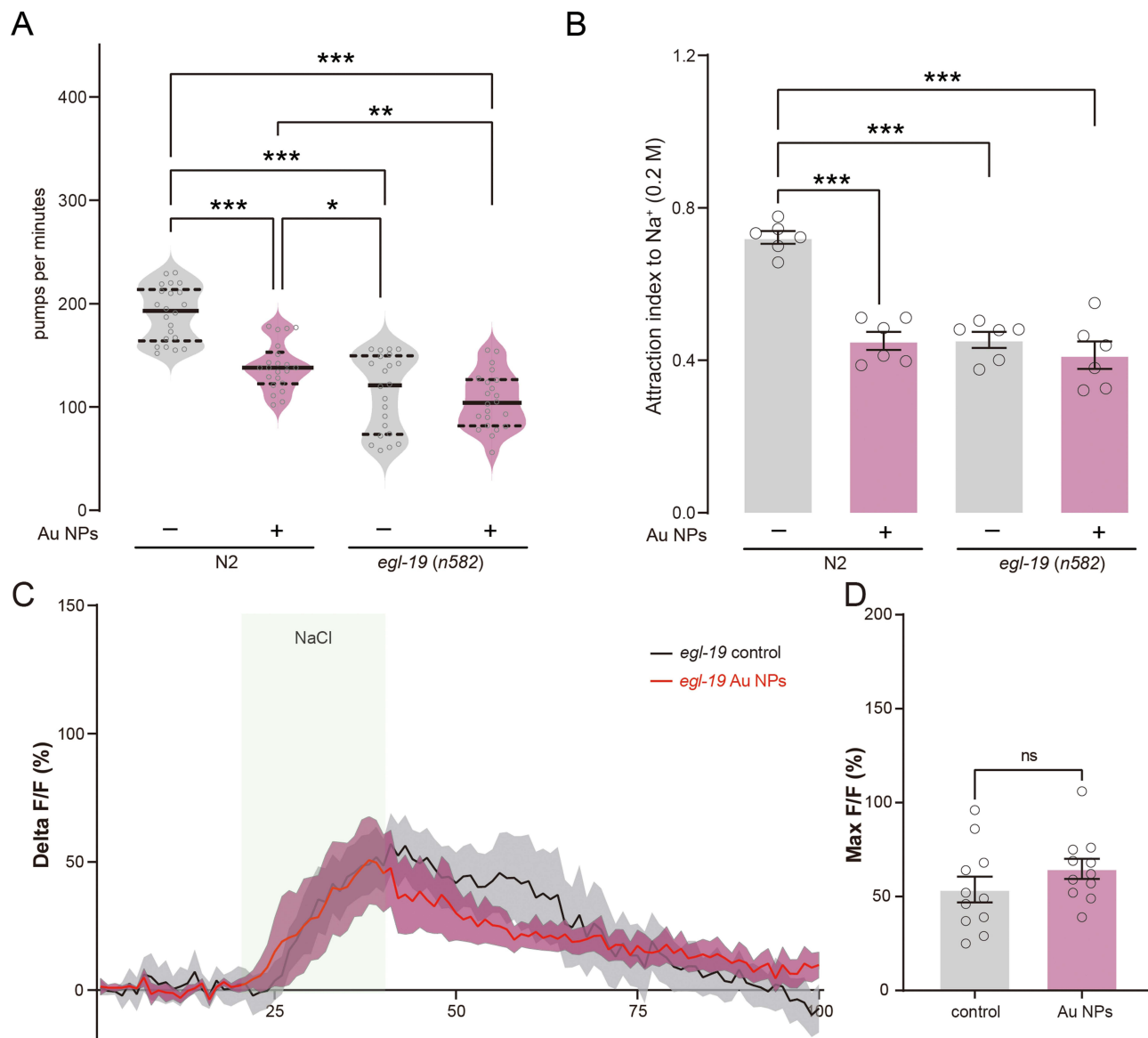


Figure 7 The voltage-gated calcium channel EGL-19 is required for Au NPs-induced calcium transit change in ASEL neurons. **(A)** The pumping rate quantification of 0 and 100 $\mu\text{g/mL}$ Au NPs-exposed wild type and *egl-19* mutant worms. **(B)** The attraction index of 0 and 100 $\mu\text{g/mL}$ Au NPs-exposed wild type and *egl-19* mutant worms to NaCl. **(C)** The calcium transit dynamics of ASEL neuron of 0 and 100 $\mu\text{g/mL}$ Au NPs-pre-exposed *egl-19* worms to 20 mM NaCl. **(D)** The max intensity of the fluorescence signal of **(C)**. Gray represents the 0 $\mu\text{g/mL}$ Au NPs group, magenta represents the 100 $\mu\text{g/mL}$ Au NPs group. Data are shown as mean \pm SE. The “ns” represents not significant. P values are represented as * $p < 0.05$, ** $p < 0.01$, *** $p < 0.001$.

calcium transit defects, the one nucleotide mutant of *egl-19* was used. This mutant ever proved a reduction in calcium transit to around 50% compared to wild type.⁷⁶ As shown in Figure 7A-D, the pumping rate and attraction index of Au NPs-treated *egl-19* mutants were not changed compared with the worms without Au NPs treatment. These results indicated that the pumping and NaCl sensation defects induced by Au NPs were dependent on *egl-19*. We further tested the calcium transit of NaCl of *egl-19* mutants treated with and without Au NPs. Consistent with the behavior assay, the real-time monitor curve of calcium transit was largely overlapped. There are no significant changes found in max florescence intensity of *egl-19* mutants with and without Au NPs treatment. These results indicated that the pumping and NaCl sensation defects induced by Au NPs are dependent on the L-type voltage-gated calcium channel EGL-19.

Conclusions

The study was focused on how the Au NPs induces neuronal gene expression changes, further causes developmental abnormality in *C. elegans*. The gene expression changes did not alter the number and morphology of neurons but affected the ASE sensory neurons' function. From the behavioral and imaging data, we demonstrated that Au NPs causes decreased calcium transit in ASEL neurons via *egl-19*. In detail, with the decreased expression of *ins-22* in ASEL neurons, the NaCl sensation was defected. Then, loss of food sensation induces less pharynx pumping. Reduced pumping rate causes less food intake. Less food intake finally causes developmental abnormality (Figure 8). Our results suggested that Au NPs could change the taste of *OP50*, which leads to the decrease in food intake, further causes developmental abnormality in animals.

Acknowledgments

This work was supported in part by grants from National Natural Science Foundation of China (22176002); Young Scientists Fund of the National Natural Science Foundation of China (82201315). Anhui Provincial Natural Science Foundation (2008085MB49); Open Project Fund of the Key Laboratory of the Ministry of Education for the Birth Population (JKZD20202); Funded Project of Anhui Medical University's Research Level Improvement Program (2021xkjT004) and Funded Project of Anhui Medical University Basic and Clinical Cooperative Research Promotion Program (2021xkjT041).

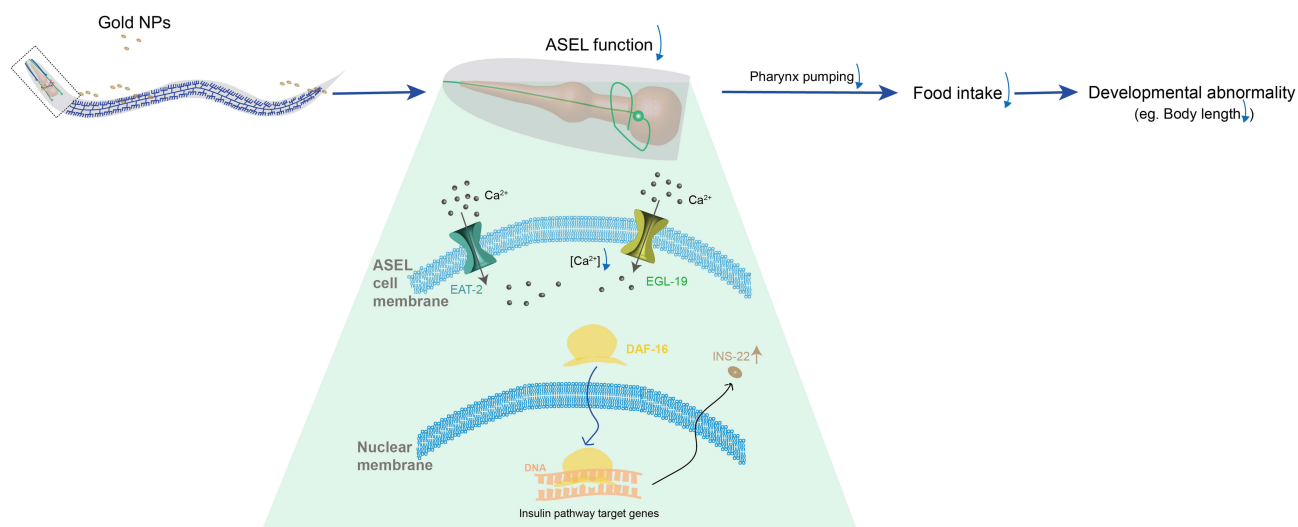


Figure 8 Schematic diagram of how *egl-19* and *eat-2* affect the functions of ASEL on chemosensation. When worms expose to a high concentration of Au NPs, it decreases the NaCl-induced intracellular calcium concentration through an *egl-19* dependent pathway, further causing the reduction of pharynx pumping, and reduces the amount of food intake. The decreased food intake causes developmental abnormality, making the worm grows slow and smaller in size.

Disclosure

The authors report no conflicts of interest.

References

1. Dragoni S, Franco G, Regoli M, et al. Gold nanoparticles uptake and cytotoxicity assessed on rat liver precision-cut slices. *Toxicol Sci.* 2012;128(1):186–197. doi:10.1093/toxsci/kfs150
2. Zhao MX, Cai ZC, Zhu BJ, Zhang ZQ. The apoptosis effect on liver cancer cells of gold nanoparticles modified with lithocholic acid. *Nanoscale Res Lett.* 2018;13:304. doi:10.1186/s11671-018-2653-8
3. Sereemasun A, Rojanathanes R, Wiwanitkit V. Effect of gold nanoparticle on renal cell: an implication for exposure risk. *Ren Fail.* 2008;30:323–325. doi:10.1080/08860220701860914
4. Nethi SK, Mukherjee S, Veeriah V, et al. Bioconjugated gold nanoparticles accelerate the growth of new blood vessels through redox signaling. *Chem Commun (Camb).* 2014;50(92):14367–14370. doi:10.1039/c4cc06996j
5. Cheng Y, Dai Q, Morshed RA, et al. Blood-brain barrier permeable gold nanoparticles: an efficient delivery platform for enhanced malignant glioma therapy and imaging. *Small.* 2014;10(24):5137–5150. doi:10.1002/sml.201400654
6. Kreyling WG, Möller W, Holzwarth U, et al. Age-dependent rat lung deposition patterns of inhaled 20 nanometer gold nanoparticles and their quantitative biokinetics in adult rats. *ACS Nano.* 2018;12(8):7771–7790. doi:10.1021/acsnano.8b01826
7. Dixit S, Novak T, Miller K, et al. Transferrin receptor-targeted theranostic gold nanoparticles for photosensitizer delivery in brain tumors. *Nanoscale.* 2015;7(5):1782–1790. doi:10.1039/c4nr04853a
8. Kim B, Han G, Toley BJ, et al. Tuning payload delivery in tumour cyndroids using gold nanoparticles. *Nat Nanotechnol.* 2010;5(6):465–472. doi:10.1038/nnano.2010.58
9. Morshed RA, Muroski ME, Dai Q, et al. Cell-penetrating peptide-modified gold nanoparticles for the delivery of doxorubicin to brain metastatic breast cancer. *Mol Pharm.* 2016;13(6):1843–1854. doi:10.1021/acs.molpharmaceut.6b00004
10. Al Hagbani T, Rizvi SMD, Hussain T, et al. Cefotaxime mediated synthesis of gold nanoparticles: characterization and antibacterial activity. *Polymers.* 2022;14(4):771. doi:10.3390/polym14040771
11. Wang L, Zheng W, Li S, Zhong L, Jiang X. Aminophenol-decorated gold nanoparticles for curing bacterial infections. *Nano Lett.* 2022;22:3576–3582. doi:10.1021/acs.nanolett.1c04968
12. Rodriguez Diaz C, Lafuente-Gómez N, Coutinho C, et al. Development of colorimetric sensors based on gold nanoparticles for SARS-CoV-2 RdRp, E and S genes detection. *Talanta.* 2022;243:123393. doi:10.1016/j.talanta.2022.123393
13. Botha TL, Boodhia K, Wepener V. Adsorption, uptake and distribution of gold nanoparticles in *Daphnia magna* following long term exposure. *Aquat Toxicol.* 2016;170:104–111. doi:10.1016/j.aquatox.2015.11.022
14. Pacheco A, Martins A, Guilhermino L. Toxicological interactions induced by chronic exposure to gold nanoparticles and microplastics mixtures in *Daphnia magna*. *Sci Total Environ.* 2018;628-629:474–483. doi:10.1016/j.scitotenv.2018.02.081
15. Porter CJ, Moghimi SM, Illum L, Davis SS. The polyoxyethylene/polyoxypropylene block co-polymer poloxamer-407 selectively redirects intravenously injected microspheres to sinusoidal endothelial cells of rabbit bone marrow. *FEBS Lett.* 1992;305:62–66. doi:10.1016/0014-5793(92)80655-z
16. Sung JH, Ji JH, Park JD, et al. Subchronic inhalation toxicity of silver nanoparticles. *Toxicol Sci.* 2009;108(2):452–461. doi:10.1093/toxsci/kfn246
17. Wiemann M, Vennemann A, Blaske F, Sperling M, Karst U. Silver nanoparticles in the lung: toxic effects and focal accumulation of silver in remote organs. *Nanomaterials.* 2017;7(12):441. doi:10.3390/nano7120441
18. Braakhuis HM, Gosens I, Krystek P, et al. Particle size dependent deposition and pulmonary inflammation after short-term inhalation of silver nanoparticles. *Part Fibre Toxicol.* 2014;11(1):49. doi:10.1186/s12989-014-0049-1
19. Zelepukin IV, Popov AA, Shipunova VO, et al. Laser-synthesized TiN nanoparticles for biomedical applications: evaluation of safety, biodistribution and pharmacokinetics. *Mater Sci Eng C Mater Biol Appl.* 2021;120:111717. doi:10.1016/j.msec.2020.111717
20. Cho WS, Cho M, Jeong J, et al. Acute toxicity and pharmacokinetics of 13 nm-sized PEG-coated gold nanoparticles. *Toxicol Appl Pharmacol.* 2009;236:16–24. doi:10.1016/j.taap.2008.12.023
21. Li X, Hu Z, Ma J, et al. The systematic evaluation of size-dependent toxicity and multi-time biodistribution of gold nanoparticles. *Colloids Surf B Biointerfaces.* 2018;167:260–266. doi:10.1016/j.colsurfb.2018.04.005
22. Semmler-Behnke M, Kreyling WG, Lipka J, et al. Biodistribution of 1.4- and 18-nm gold particles in rats. *Small.* 2008;4(12):2108–2111. doi:10.1002/sml.200800922
23. Tsyusko OV, Unrine JM, Spurgeon D, et al. Toxicogenomic responses of the model organism *Caenorhabditis elegans* to gold nanoparticles. *Environ Sci Technol.* 2012;46(7):4115–4124. doi:10.1021/es2033108
24. Papastefanaki F, Jakovcevski I, Poulia N, et al. Intraspinal delivery of polyethylene glycol-coated gold nanoparticles promotes functional recovery after spinal cord injury. *Mol Ther.* 2015;23(6):993–1002. doi:10.1038/mt.2015.50
25. Lin YL, Jen JC, Hsu SH, Chiu IM. Sciatic nerve repair by microgrooved nerve conduits made of chitosan-gold nanocomposites. *Surg Neurol.* 2008;70:9–18. doi:10.1016/j.surneu.2008.01.057
26. Bhang SH, Han J, Jang H-K, et al. pH-triggered release of manganese from MnAu nanoparticles that enables cellular neuronal differentiation without cellular toxicity. *Biomaterials.* 2015;55:33–43. doi:10.1016/j.biomaterials.2015.03.025
27. Carvalho-de-Souza JL, Treger J, Dang B, et al. Photosensitivity of neurons enabled by cell-targeted gold nanoparticles. *Neuron.* 2015;86(1):207–217. doi:10.1016/j.neuron.2015.02.033
28. Das S, Sharma M, Saharia D, et al. In vivo studies of silk based gold nano-composite conduits for functional peripheral nerve regeneration. *Biomaterials.* 2015;62:66–75. doi:10.1016/j.biomaterials.2015.04.047
29. Das M, Shim KH, An SSA, Yi DK. Review on gold nanoparticles and their applications. *Toxicol Environ Health Sci.* 2011;3:193–205. doi:10.1007/s13530-011-0109-y
30. Yen HJ, Hsu SH, Tsai CL. Cytotoxicity and immunological response of gold and silver nanoparticles of different sizes. *Small.* 2009;5:1553–1561. doi:10.1002/sml.200900126

31. Kang B, Mackey MA, El-Sayed MA. Nuclear targeting of gold nanoparticles in cancer cells induces DNA damage, causing cytokinesis arrest and apoptosis. *J Am Chem Soc.* 2010;132:1517–1519. doi:10.1021/ja9102698
32. Pan Y, Leifert A, Ruau D, et al. Gold nanoparticles of diameter 1.4 nm trigger necrosis by oxidative stress and mitochondrial damage. *Small.* 2009;5(18):2067–2076. doi:10.1002/smll.200900466
33. Li JJ, Hartono D, Ong CN, Bay BH, Yung LYL. Autophagy and oxidative stress associated with gold nanoparticles. *Biomaterials.* 2010;31:5996–6003. doi:10.1016/j.biomaterials.2010.04.014
34. Leung MC, Williams PL, Benedetto A, et al. *Caenorhabditis elegans*: an emerging model in biomedical and environmental toxicology. *Toxicol Sci.* 2008;106(1):5–28. doi:10.1093/toxsci/kfn121
35. Wang J, Wang L, Zhao W, et al. The role of apoptosis pathway in the cytotoxicity induced by fresh and aged zinc oxide nanoparticles. *Nanoscale Res Lett.* 2021;16(1). doi:10.1186/s11671-021-03587-y
36. Lei W, Min W, Hui D, Yun L, An X. Effect of surface modification on cellular internalization of Fe₃O₄ nanoparticles in strong static magnetic field. *J Nanosci Nanotechnol.* 2015;15:5184–5192. doi:10.1166/jnn.2015.9841
37. Wang L, Wang M, Du H, Liu Y, Xu A. Lipid metabolism was interfered by phosphatidylcholine-coated magnetic nanoparticles in *C. elegans* exposed to 0.5 T static magnetic field. *J Nanosci Nanotechnol.* 2017;17:3172–3180. doi:10.1166/jnn.2017.13051
38. Lei W, Beaudoin-Chabot C, Thibault G. Glucose increases the lifespan of post-reproductive *C. elegans* independently of FOXO. *bioRxiv.* 2018;347435.
39. Wang L, Du H, Guo X, et al. Developmental abnormality induced by strong static magnetic field in *Caenorhabditis elegans*. *Bioelectromagnetics.* 2015;36(3):178–189. doi:10.1002/bem.21906
40. Beaudoin-Chabot C, Wang L, Celik C, et al. The unfolded protein response reverses the effects of glucose on lifespan in chemically-sterilized *C. elegans*. *Nat Commun.* 2022;13(1):5889. doi:10.1038/s41467-022-33630-0
41. Tsyusko OV, Unrine JM, Spurgeon D, et al. Toxicogenomic responses of the model organism *Caenorhabditis elegans* to gold nanoparticles. *Environ Sci Technol.* 2012;46(7):4115–4124. doi:10.1021/es2033108
42. McElwee JJ, Schuster E, Blanc E, Thomas JH, Gems D. Shared transcriptional signature in *Caenorhabditis elegans* Dauer larvae and long-lived daf-2 mutants implicates detoxification system in longevity assurance. *J Biol Chem.* 2004;279:44533–44543. doi:10.1074/jbc.M406207200
43. Qin Zhu JIM, Tan K, Kim J. qinZhu/VisCello: visCello v1.0.0 (v1.0.0). *Science.* 2019;365:eax1971. doi:10.5281/zenodo.3262313
44. Bargmann CI, Horvitz HR. Chemosensory neurons with overlapping functions direct chemotaxis to multiple chemicals in *C. elegans*. *Neuron.* 1991;7:729–742. doi:10.1016/0896-6273(91)90276-6
45. Bargmann CI, Hartweg E, Horvitz HR. Odorant-selective genes and neurons mediate olfaction in *C. elegans*. *Cell.* 1993;74(3):515–527. doi:10.1016/0092-8674(93)80053-h
46. Troemel ER, Chou JH, Dwyer ND, Colbert HA, Bargmann CI. Divergent seven transmembrane receptors are candidate chemosensory receptors in *C. elegans*. *Cell.* 1995;83(2):207–218. doi:10.1016/0092-8674(95)90162-0
47. Wang L, Graziano B, Encalada N, et al. Glial regulators of ions and solutes required for specific chemosensory functions in *Caenorhabditis elegans*. *iScience.* 2022;25(12):105684. doi:10.1016/j.isci.2022.105684
48. Rueden CT, Schindelin J, Hiner MC, et al. ImageJ2: imageJ for the next generation of scientific image data. *BMC Bioinform.* 2017;18(1):529. doi:10.1186/s12859-017-1934-z
49. Lim JP, Fehlauer H, Das A, et al. Loss of CaMKI function disrupts salt aversive learning in *C. elegans*. *J Neurosci.* 2018;38(27):6114–6129. doi:10.1523/JNEUROSCI.1611-17.2018
50. Edelstein AD, Tsuchida MA, Amodaj N, et al. Advanced methods of microscope control using muManager software. *J Biol Methods.* 2014;1(2):e10. doi:10.14440/jbm.2014.36
51. Warde-Farley D, Donaldson SL, Comes O, et al. The GeneMANIA prediction server: biological network integration for gene prioritization and predicting gene function. *Nucleic Acids Res.* 2010;38(suppl_2):W214–220. doi:10.1093/nar/gkq537
52. Szklarczyk D, Gable AL, Lyon D, et al. STRING v11: protein-protein association networks with increased coverage, supporting functional discovery in genome-wide experimental datasets. *Nucleic Acids Res.* 2019;47(D1):D607–D613. doi:10.1093/nar/gky1131
53. Kim IY, Joachim E, Choi H, Kim K. Toxicity of silica nanoparticles depends on size, dose, and cell type. *Nanomedicine.* 2015;11:1407–1416. doi:10.1016/j.nano.2015.03.004
54. Coradeghini R, Gloria S, Garcia CP, et al. Size-dependent toxicity and cell interaction mechanisms of gold nanoparticles on mouse fibroblasts. *Toxicol Lett.* 2013;217(3):205–216. doi:10.1016/j.toxlet.2012.11.022
55. Mironava T, Hadjiargyrou M, Simon M, Jurukovski V, Rafailovich MH. Gold nanoparticles cellular toxicity and recovery: effect of size, concentration and exposure time. *Nanotoxicology.* 2010;4:120–137. doi:10.3109/17435390903471463
56. Kim TH, Kim M, Park H-S, et al. Size-dependent cellular toxicity of silver nanoparticles. *J Biomed Mater Res A.* 2012;100(4):1033–1043. doi:10.1002/jbm.a.34053
57. Kim KT, Zaikova T, Hutchison JE, Tanguay RL. Gold nanoparticles disrupt zebrafish eye development and pigmentation. *Toxicol Sci.* 2013;133:275–288. doi:10.1093/toxsci/kft081
58. Browning LM, Lee KJ, Huang T, et al. Random walk of single gold nanoparticles in zebrafish embryos leading to stochastic toxic effects on embryonic developments. *Nanoscale.* 2009;1(1):138–152. doi:10.1039/b9nr00053d
59. Avery L, You YJC. *Elegans* feeding. *WormBook.* 2012;1–23. doi:10.1895/wormbook.1.150.1
60. Raizen DM, Lee RY, Avery L. Interacting genes required for pharyngeal excitation by motor neuron MC in *Caenorhabditis elegans*. *Genetics.* 1995;141:1365–1382. doi:10.1093/genetics/141.4.1365
61. Abdelhalim MA, Mady MM. Liver uptake of gold nanoparticles after intraperitoneal administration in vivo: a fluorescence study. *Lipids Health Dis.* 2011;10:195. doi:10.1186/1476-511X-10-195
62. Balasubramanian SK, Jititiwat J, Manikandan J, et al. Biodistribution of gold nanoparticles and gene expression changes in the liver and spleen after intravenous administration in rats. *Biomaterials.* 2010;31(8):2034–2042. doi:10.1016/j.biomaterials.2009.11.079
63. Li X, Wang B, Zhou S, et al. Surface chemistry governs the sub-organ transfer, clearance and toxicity of functional gold nanoparticles in the liver and kidney. *J Nanobiotechnology.* 2020;18(1):45. doi:10.1186/s12951-020-00599-1
64. Isoda K, Tanaka A, Fuzimori C, et al. Toxicity of gold nanoparticles in mice due to nanoparticle/drug interaction induces acute kidney damage. *Nanoscale Res Lett.* 2020;15(1):141. doi:10.1186/s11671-020-03371-4

65. Ibrahim KE, Al-Mutary MG, Bakhiet AO, Khan HA. Histopathology of the liver, kidney, and spleen of mice exposed to gold nanoparticles. *Molecules*. 2018;23:1848. doi:10.3390/Molecules23081848
66. Abdelhalim MA, Abdelmottaleb Moussa SA. The gold nanoparticle size and exposure duration effect on the liver and kidney function of rats: in vivo. *Saudi J Biol Sci*. 2013;20:177–181. doi:10.1016/j.sjbs.2013.01.007
67. Albeg A, Smith CJ, Chatzigeorgiou M, et al. C. elegans multi-dendritic sensory neurons: morphology and function. *Mol Cell Neurosci*. 2011;46(1):308–317. doi:10.1016/j.mcn.2010.10.001
68. Singhvi A, Liu B, Friedman C, et al. A Glial K/Cl transporter controls neuronal receptive ending shape by chloride inhibition of an rGC. *Cell*. 2016;165(4):936–948. doi:10.1016/j.cell.2016.03.026
69. Galletti F, Strazzullo P, Ferrara I, et al. NaCl sensitivity of essential hypertensive patients is related to insulin resistance. *J Hypertens*. 1997;15(12):1485–1491. doi:10.1097/00004872-199715120-00017
70. Oda S, Tomioka M, Iino Y. Neuronal plasticity regulated by the insulin-like signaling pathway underlies salt chemotaxis learning in *Caenorhabditis elegans*. *J Neurophysiol*. 2011;106:301–308. doi:10.1152/jn.01029.2010
71. Burton NO, Furuta T, Webster AK, et al. Insulin-like signalling to the maternal germline controls progeny response to osmotic stress. *Nat Cell Biol*. 2017;19(3):252–257. doi:10.1038/ncb3470
72. Minniti AN, Arriagada H, Zúñiga S, et al. Temporal pattern of neuronal insulin release during *Caenorhabditis elegans* aging: role of redox homeostasis. *Aging Cell*. 2019;18(1):e12855. doi:10.1111/ace1.12855
73. Pierce SB, Costa M, Wisotzkey R, et al. Regulation of DAF-2 receptor signaling by human insulin and ins-1, a member of the unusually large and diverse C. elegans insulin gene family. *Genes Dev*. 2001;15(6):672–686. doi:10.1101/gad.867301
74. Leinwand SG, Chalasani SH. Neuropeptide signaling remodels chemosensory circuit composition in *Caenorhabditis elegans*. *Nat Neurosci*. 2013;16:1461–1467. doi:10.1038/nn.3511
75. Frokjaer-Jensen C, Kindt KS, Kerr RA, et al. Effects of voltage-gated calcium channel subunit genes on calcium influx in cultured C. elegans mechanosensory neurons. *J Neurobiol*. 2006;66(10):1125–1139. doi:10.1002/neu.20261
76. Duan D, Zhang H, Yue X, et al. Sensory glia detect repulsive odorants and drive olfactory adaptation. *Neuron*. 2020;108(4):707–721 e708. doi:10.1016/j.neuron.2020.08.026
77. Shindou T, Ochi-Shindou M, Murayama T, et al. Active propagation of dendritic electrical signals in C. elegans. *Sci Rep*. 2019;9(1):3430. doi:10.1038/s41598-019-40158-9
78. Shtonda B, Avery L. CCA-1, EGL-19 and EXP-2 currents shape action potentials in the *Caenorhabditis elegans* pharynx. *J Exp Biol*. 2005;208:2177–2190. doi:10.1242/jeb.01615

International Journal of Nanomedicine

Dovepress

Publish your work in this journal

The International Journal of Nanomedicine is an international, peer-reviewed journal focusing on the application of nanotechnology in diagnostics, therapeutics, and drug delivery systems throughout the biomedical field. This journal is indexed on PubMed Central, MedLine, CAS, SciSearch®, Current Contents®/Clinical Medicine, Journal Citation Reports/Science Edition, EMBase, Scopus and the Elsevier Bibliographic databases. The manuscript management system is completely online and includes a very quick and fair peer-review system, which is all easy to use. Visit <http://www.dovepress.com/testimonials.php> to read real quotes from published authors.

Submit your manuscript here: <https://www.dovepress.com/international-journal-of-nanomedicine-journal>